Industrial Robot Accuracy Degradation Monitoring and Quick Health Assessment

Guixiu Qiao[1]
Mem. ASME
National Institute of Standards and Technology,
100 Bureau Drive,
Gaithersburg, MD 20899
e-mail: guixiu.qiao@nist.gov

Brian A. Weiss
Mem. ASME
National Institute of Standards and Technology,
100 Bureau Drive,
Gaithersburg, MD 20899
e-mail: brian.weiss@nist.gov

Robot accuracy degradation sensing, monitoring, and assessment are critical activities in many industrial robot applications, especially when it comes to the high accuracy operations which may include welding, material removal, robotic drilling, and robot riveting. The degradation of robot tool center accuracy can increase the likelihood of unexpected shutdowns and decrease manufacturing quality and production efficiency. The development of monitoring, diagnostic and prognostic (collectively known as prognostics and health management (PHM)) technologies can aid manufacturers in maintaining the performance of robot systems. PHM can provide the techniques and tools to support the specification of a robot's present and future health state and optimization of maintenance strategies. This paper presents the robotic PHM research and the development of a quick health assessment at the U.S. National Institute of Standards and Technology (NIST). The research effort includes the advanced sensing development to measure the robot tool center position and orientation; a test method to generate a robot motion plan; an advanced robot error model that handles the geometric/nongeometric errors and the uncertainties of the measurement system, and algorithms to process measured data to assess the robot's accuracy degradation. The algorithm has no concept of the traditional derivative or gradient for algorithm converging. A use case is presented to demonstrate the feasibility of the methodology. [DOI: 10.1115/1.4043649]

1 Introduction

Increasingly accurate, cost-effective, and flexible robot technologies are accelerating robot adoption going beyond the repetitive, high-volume production tasks [1–3]. Small batches and customized production are common in current robot work cells that require design changes and variants. Traditional teaching methods are becoming obsolete because they are time-consuming and unique (e.g., drilling thousands of holes on an airplane's fuselage) [4]. Manufacturers are promoting robots' enhanced capability to achieve accuracy improvement [5,6]. Improved accuracy allows robot technologies to enable more robot offline programing that leads to significant time and cost savings [7]. This emergent capability also allows robot technologies to be used across broader applications, including assembly, high accuracy welding, material removal, robot machining, medical operations, and robot 3D printing [8–11]. High accuracy robots are becoming valuable tools for many of the afore-mentioned processes because of the substantial cost savings that can be achieved through these new technological integrations [4,11]. The recent demand for high accuracy robot-in-manufacturing processes has increased the importance of robot accuracy sensing, degradation monitoring, and assessment research.

Degradations in robot accuracy are less observable compared to system freezes or shutdowns. When a robot's accuracy is degrading, the robot may still be operating, but it is likely working at a decreased level of productivity and/or outputting products of reduced quality [3]. There are many influences on the position and orientation accuracy of the robot's tool center point (TCP). Changes, even small or subtle, to the joint components or the component relationships can compromise TCP accuracy. The initial kinematic parameters defined within the robot's controller will become less reflective of the robot's true geometry as physical degradations manifest. Thermal expansion, gear error due to degradation, and structural deformation can cause TCP accuracy degradation that will compromise the manufacturing system's ability to meet its target goals.

Most existing research on assessing robot TCP accuracy degradation is focused on robot arm component failures. In the scope of this research effort, components are defined as constituent elements that comprise the robot arm (e.g., joints, motors, gears, and encoders) [12–17]. For example, there is research aimed at monitoring gear wear [12], assessing joint failures [13,17], or analyzing electronic board failures [14]. Given the complexity of the robot arm, it is challenging to determine the constituent elements' specific influences on the arm's overall performance. Measuring the accuracy of a single joint is not a complete representation of the robot's final TCP accuracy. In many cases, the TCP accuracy degradations come from changing relationships between components, for example, the change of squareness between links. Furthermore, component assessments largely depend upon historical data. When the configuration or operational parameter changes, e.g., changing payload, the assessment criteria for the abnormal status may change too. A solution is needed from the system level using the exact TCP accuracy to assess if the degradation is still within the specification required by the application.

Monitoring, diagnostic, and prognostic technologies (collectively known as prognostics and health management (PHM)) have emerged as a means to aid manufacturers in assessing robot health and optimizing the maintenance of robot systems. Robot arm accuracy degradation PHM is one of the important research areas within the robotics domain [16,17]. A quick health assessment methodology was developed to enable manufacturers to quickly assess a robot's accuracy degradation throughout the robot workspace. This effort constitutes a subset of research in the Prognostics, Health Management, and Control project at the National Institute of Standards and Technology (NIST) [14].

In this paper, the overview section gives an introduction of the quick health assessment methodology. A workflow shows the key procedures of the robot accuracy degradation assessment. The following sections detail the developments of the key procedures in the workflow. They include the development of robot measurement plan, a test method model, and algorithms to solve the test method

[1]Corresponding author.

Manuscript received March 18, 2019; final manuscript received April 26, 2019; published online May 14, 2019. Assoc. Editor: Y. Lawrence Yao.

model. The paper concludes with the discussion of a use case to demonstrate the feasibility of the methodology.

2 Overview of the Quick Health Assessment Methodology

Research is being conducted at NIST to develop performance metrics, test methods, reference datasets, and supporting tools that the manufacturing community can leverage to enhance their PHM capabilities [18,19]. NIST researchers have developed a quick health assessment methodology to assess the robot tool center accuracy degradation throughout a robot's workspace. The purpose is to enhance maintenance and control strategies within robotic operations that can also inform upon workcell operations.

The methodology includes: (1) the development of an advanced sensor to measure the robot tool center positions and orientations, (2) a test method to define the robot movements, (3) a robot error model to reflect the robot geometric and nongeometric errors, and (4) algorithms to process measured data to assess the robot's health.

Figure 1 shows the workflow of the quick health assessment methodology. First, a robot measurement plan is generated to guide the robot measurement. The measurement plan needs to satisfy the requirements of the test method model (will be detailed in Sec. 3). Then, the robot is commanded to move based on the measurement plan. During the movement, a vision-based 7D measurement system is used to measure the robot TCP's position (x, y, and z) and orientation (pitch, yaw, and roll). The output of the 7D measurement system is time, x, y, z, pitch, yaw, and roll. This advanced sensor, developed at NIST, is patent pending and will not be detailed in this paper (see prior publication [20] for additional publicly available information). Then, the measured data are inputted to the test method model and the analysis algorithms. The test method model creates a robot error model that can represent robot's position-dependent, nongeometric errors, such as the nonideal motion of joints or deflections of the robot's structure. A novel algorithm is developed to solve the robot error model that contains hundreds of unidentified parameters. A method is developed to decouple the measurement instrument's uncertainties from the actual robot errors. The analysis outputs the accuracy degradation assessment results.

The quick health assessment methodology addresses the following challenges:

- Measuring the actual robot positions and orientations with less interruption of production using a noncontact measurement system in between manufacturing operations.
- Assessing the robot tool center errors in a volumetric way. A robot could have multiple inverse kinematic solutions to reach a location in a Cartesian space. As a result, the error magnitude and direction can change when using different inverse kinematic solutions. This makes the assessment of the tool center accuracy difficult since it is difficult to measure the accuracy from all directions.
- Assessing the robot's overall health using limited measurements. It is impossible to take unlimited measurements to assess the robot's accuracy degradation over the entire workspace using all possible arm poses.
- Decoupling the measurement instrument's uncertainty from the actual robot errors. If the uncertainties of the measurement instrument are usually treated as joint errors, the assessment results may be biased [21].

The goal of the quick health assessment methodology is to enable manufacturers to assess a robot's tool center accuracy degradation in as little as 10 min (depending upon the necessary motion path and work volume). The quick health assessment methodology can detect TCP accuracy degradations stemming from changes of environmental conditions, workcell reconfigurations, or components degrading within the robotic arm. The methodology will monitor the degradation of robot performance leading to reducing unexpected shutdowns and supporting the optimization of maintenance strategies to improve productivity.

This paper focuses on the development of algorithms to use the limited sample measurement to assess the robot accuracy degradation in the overall robot measurement volume. In Sec. 3, the algorithm to develop the fixed-loop measurement plan is presented.

3 Fixed-Loop Measurement Plan Generation

A measurement plan is needed to command the robot motions. The commanded robot motions for the accuracy degradation assessment cannot be arbitrary movements. The measurement plan requires the robot TCP to move throughout the entire workspace and need to be evenly distributed in both joint space and Cartesian space. The even distribution of sampling prevents the analysis algorithm from missing errors or too heavily weighting errors, which will bias the results. The coverage of overall joint space and Cartesian space means that the measurement plan will exercise the robot beyond a partial range of joints or work zones. It enables the capture of joint performance through the overall motor and encoder ranges. Covering the entire workspace enables the evaluation of various rigidity conditions. To minimize potential interruptions during robot motion and measurement, a collision check is performed when the measurement plan is generated. Also, a line-of-sight check is implemented to ensure the planned positions are not visually occluded positions from the measurement instrument.

A use case was developed using a UR5 by Universal Robotics. The fixed-loop motion generated for the UR5 is shown in Fig. 2. The left picture shows the initial generation of the measurement plan that assumes an unimpeded work volume. The right picture shows the fixed-loop motion that passes all the checks required by the test method. Because the UR5 robot was mounted on an optical table, only poses above the table are valid for this use case. The robot motion assumes an unimpeded work volume above the table.

Figure 3 shows the flowchart of the fixed-loop measurement plan generation. Step 1 begins with generating a set of randomly

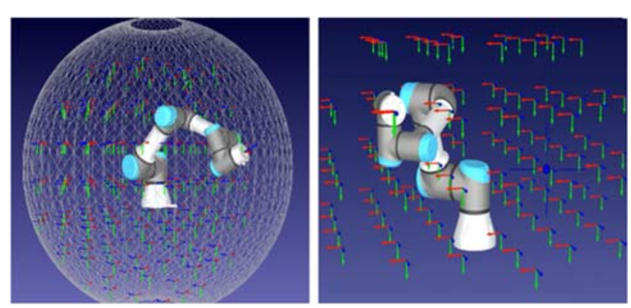

Fig. 2 Fixed-loop measurement plan for UR5

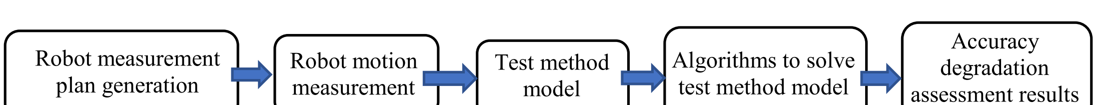

Fig. 1 Workflow of the robot accuracy degradation quick assessment methodology

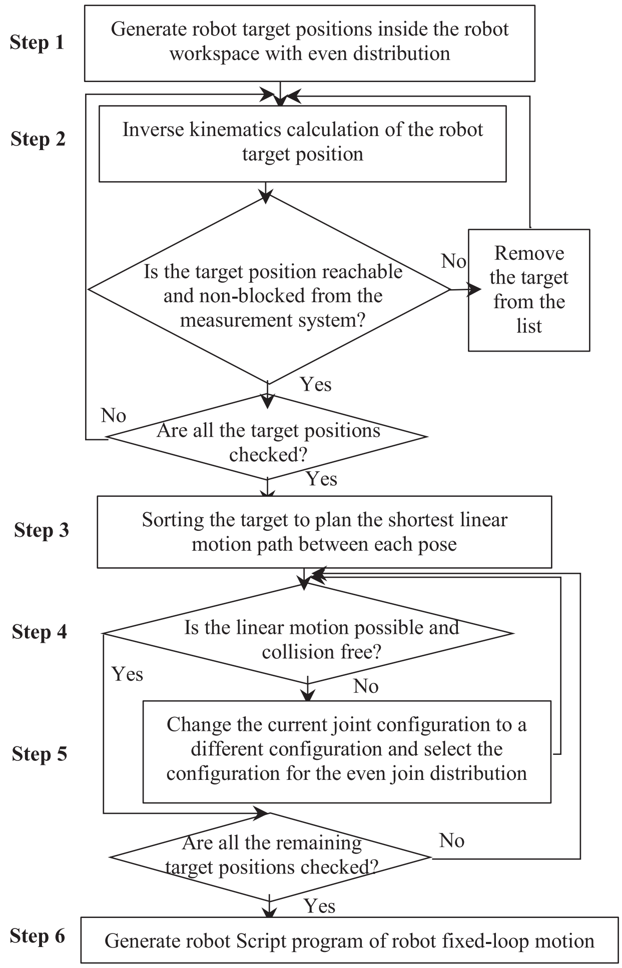

Fig. 3 Robot fixed-loop motion generation flowchart

distributed robot locations in Cartesian space within the robot's work volume. The inverse kinematics is calculated in step 2 to determine if each target position has an inverse kinematics solution. If the Cartesian position of the 7D measurement system relative to the robot is known, a line-of-sight check is performed to ensure that the smart target is visible to the measurement system. If these conditions are not satisfied, the target position is removed from the list of viable points. After all the target positions are checked, step 3 performs a sorting algorithm to plan the shortest linear motion path between each pose. A measurement plan that contains fewer "back and forth" motions is more efficient to decrease the overall times for robot movements and measurements. Step 4 performs checks to determine if the linear motion between adjacent points is plausible and if collisions will occur along the path. Since each pose in the space has multiple inverse kinematics solutions to convert it into joint angles, the current joint configuration is changed to a different configuration and check again if collisions are predicted. Step 5 selects the configuration that can satisfy the even joint distribution requirement. This pose is then added as one of the target locations in the fixed-loop motion. Otherwise, if there is no configuration to satisfy the linear motion, the linear path is replaced by a curved motion path. If a curved motion path is not possible, this target pose is skipped. The reason linear motion paths are preferred is that additional analyses can be performed. For example, angle errors can also be found between the linear lines. Error patterns can be analyzed from the line fitting results. Steps 4 and 5 are repeated until all the paths are evaluated. A robot Script program of the robot fixed-loop motion is generated during step 6. The fixed-loop motion is copied to the robot controller.

The fixed-loop measurement plan will be executed periodically. The initial setup includes downloading the fixed-loop measurement plan to the robot controller, preparing the measurement software, mounting the smart target on the robot end effector, and setup the measurement instrument on the floor. The smart target can be kept on the end effector for repeat measurements. It takes a relatively short amount of time to measure the robot moving on the fix-loop measurement plan. While the robot tool center is moving to these predetermined positions, measurements are taken from the 7D measurement system developed at NIST [22]. Outputs from the measurement system are time, x, y, z, pitch, yaw, and roll (of the robot TCP). Measurement data are the input of the test method model and are used to identify the parameters of the test method model.

4 Test Method Model to Represent the Position-Dependent Robot Errors

In the measurement process of the quick health assessment methodology, a limited amount of robot arm poses is measured. However, a robot may work at different locations within its workspace using different poses from the measurement plan. Since only limited sample locations are measured, the location where the minimum or maximum degradation occurs may not be included in the sample measurements. A model is needed to represent the robot errors.

It is well known that if a machine or instrument is not repeatable, it cannot be calibrated or modeled to represent the errors since errors are not repeatable [23]. Because robots are highly repeatable instruments, calibration or modeling is feasible but needs to handle complex errors. Traditional modeling methods for robot errors assume that the robot can be represented as a set of rigid links connected by ideal motion joints. When a robot joint motion is ideal, the geometric relationships between the joints are constant [21]. Errors are constant offsets of geometric relationships coming from the as-built structures and joints deviating from the design specifications. In reality, robot joint motion is not ideal. There exist nongeometric errors between successive joints, such as the nonideal motion of joints, and deflections of the structure and joints due to external loading, gravity, backlash, etc. Recent researches have added the consideration of backlash errors, etc. [24–26]. Since these errors are not constant values, they need to be treated as position-dependent errors.

An advanced error model is developed at NIST for the quick health assessment methodology. The error model enables the characterization of position-dependent errors. It can also handle nongeometric errors, such as the nonideal motion of joints and deflections of the structure and joints.

Parameters that describe the geometric relationships are not constant values anymore. They are functions of the axis locations. Any error of the joint axis will be reflected in the TCP errors throughout the kinematic chain. Figure 4 shows the general errors of a rotary axis (i-axis), which represents the ith joint of a robot. In Fig. 4, the real axis has deviated from its designed position. The reason for the deviation could be from the errors in robot geometry, axis motion, robot gear box degradation, backlash, thermal environment changes, or external loading [25]. Each of the six robot joint axes contains six axis errors: three translation errors (δ_x, δ_y, and δ_z in x, y, and z directions) and three rotation errors (ε_x, ε_y, and ε_z as pitch, yaw, and roll). δ_x is the radial error motion of the ith-axis in the X direction; δ_y is the radial error motion of the ith-axis in the Y direction; δ_z is the axial error motion of the ith-axis in the Z direction; ε_x represents tilt error motion around X of the ith-axis; ε_y represents tilt error motion around Y of the ith-axis; and ε_z represents angular positioning error around Z of the ith-axis. ε_z is also called the scale error of the rotation axis. The error model of the joint is described in Eq. (1). $E_{(i-1)i}$ is the transformation from frame $i-1$ to frame i, and θ is the ith joint angle variable. The $\delta(\theta)$ and $\varepsilon(\theta)$ in Eq. (1) are not constant values as is typical in traditional modeling methods. They are functions of

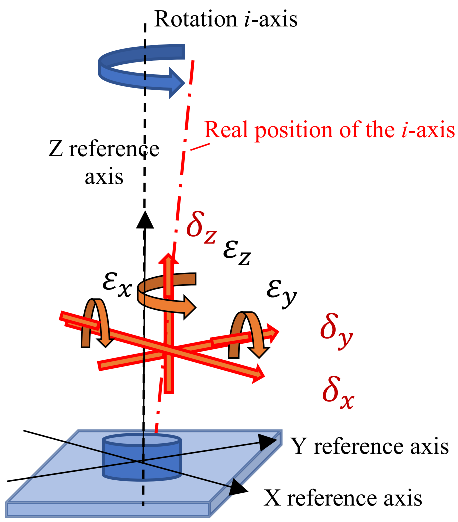

Fig. 4 Six degree-of-freedom errors of the rotation axis

joint positions.

$$E_{(i-1)i}(\theta) = \begin{bmatrix} 1 & -\varepsilon_z(\theta) & \varepsilon_y(\theta) & \delta_x(\theta) \\ \varepsilon_z(\theta) & 1 & -\varepsilon_x(\theta) & \delta_y(\theta) \\ -\varepsilon_y(\theta) & \varepsilon_x(\theta) & 1 & \delta_z(\theta) \\ 0 & 0 & 0 & 1 \end{bmatrix} \quad (1)$$

To describe errors as the function of joint positions, base functions are needed for the $\varepsilon_x(\theta)$, $\varepsilon_y(\theta)$, $\varepsilon_z(\theta)$, $\delta_x(\theta)$, $\delta_y(\theta)$, and $\delta_z(\theta)$ to represent the general position-dependent axis errors. The Chebyshev polynomial is selected [26] as the solution of the base function because of the two advantages [26,27]. They are: (1) Chebyshev polynomials are orthogonal to each other over an interval and (2) Chebyshev polynomials all have a similar scale over the same interval. Using this base function definition, the $\delta(\theta)$ and $\varepsilon(\theta)$ in Eq. (1) are presented as high-order position-dependent polynomials with unknown polynomial coefficients

$$\delta_x(\hat{\theta}) = a_0 + a_1 c_1(\hat{\theta}) + a_2 c_2(\hat{\theta}) + \cdots + a_m c_m(\hat{\theta}) \quad (2)$$

$$\varepsilon_x(\hat{\theta}) = b_0 + b_1 c_1(\hat{\theta}) + b_2 c_2(\hat{\theta}) + \cdots + b_m c_m(\hat{\theta}) \quad (3)$$

where $\hat{\theta}_i = a_0((2(\theta_i - \theta_{i,\min}))/((\theta_{i,\max} - \theta_{i,\min}))) - 1$ denotes the mapping of the ith linearly joint command θ_i, where the joint range is $[\theta_{i,\min}\ \theta_{i,\max}]$, being scaled to the interval $[-1\ 1]$. $\theta_{i,\min}$ and $\theta_{i,\max}$ are the minimum and maximum joint angles. Also, a_i is the gain on ith basis function and $c_i(\hat{\theta})$ is the ith basis function.

$$\text{Where } c_0(\hat{\theta}) = 1, \quad c_1(\hat{\theta}) = \theta, \quad c_2(\hat{\theta}) = 2\hat{\theta}^2 - 1$$

$$c_3(\hat{\theta}) = 4\hat{\theta}^3 - 3\hat{\theta}, \quad C_{m+1}(\hat{\theta}) = 2\theta C_m(\hat{\theta}) - C_{m-1}(\hat{\theta})$$

Thus, the zero-order term (the constant offsets) in the equation can be regarded as the constant error description for joint $i-1$, and other high-order terms are the position-dependent errors for joint i.

Equation (1) is the general representation of all the errors between the nominal transformation matrices. The complete kinematic model, including errors, is described as

$$F_{\text{forward}} = E_0 A_0^1 E_{01} A_1^2 E_{12} A_2^3 E_{23} \cdots A_{n-1}^n E_{(n-1)n} \quad (4)$$

where A is the nominal axis motion, A_0^1 is the nominal transformation from joint 0 to joint 1, E is the error of the joint, E_0 is the setup error of the robot base, and E_{01} is the transformation error from joint 0 to joint 1.

The next challenge is how to decouple measurement uncertainties from the real robot errors. If the uncertainties of the measurement instrument are treated as joint errors, the assessment results may be biased. An implicit loop method is implemented to decouple the 7D measurement system's measurement uncertainties from the actual robot errors [28]. This method treats the robot as having a closed kinematic chain, with the 7D measurement system included in the kinematic chain. In the implicit loop method, the first link (referred to as the base link) extends to the TCP, then connects to the measuring device (i.e., 7D measurement system), and then loops back to the base link. These connections form a closed loop. The displacements around a closed loop sum to zero which is mathematically represented as the identity matrix. With this convention, the 7D measurement system's uncertainty is characterized inside the modeling equation using a weight. The kinematic model of the robot is

$$I = E_0 A_0^1 E_{01} A_1^2 E_{12} A_2^3 E_{23} \cdots A_{n-1}^n E_{(n-1)n} A_n^0 E_{n0} \quad (5)$$

Given the example of a UR5 containing six joints, there are six joints-worth of E matrices plus a base E matrix and a tool E matrix, providing eight E matrices that need to be solved. Each E matrix has six Chebyshev polynomials. The order of the polynomials should be large enough to capture the dominant error characteristics. Usually, a fifth or sixth order polynomial is sufficient to capture the error characteristics for robot motion. Given the condition of using fifth orders, each E has at least 36 unknown parameters. Overall, there are at least 288 parameters that need to be identified by the analysis algorithm.

5 Optimization Algorithm for Parameter Identification

To assess the robot accuracy degradation, the model parameter coefficients need to be identified. The robot is treated as a high-dimensional system with unknown parameters. The complete parameter list now is the unknown coefficients of the polynomials of the error terms in each of the E matrices. Because the Chebyshev polynomial base functions are orthogonal to each other over an interval, the challenge is solved of decoupling zero-order and high-order errors when introducing high-order errors in parameter identification.

The solution to this problem is the development of the nonlinear optimization method. All measurements from the 7D measurement instrument, joint and measuring device, are placed in a single measurement vector x. Equation (5) becomes

$$\begin{aligned} &f(x,p) = 0 \quad f: R^k \times R^n \to R^m \\ &x \in R^k, \quad p \in R^n, \quad f \in R^m \end{aligned} \quad (6)$$

In Eq. (6), x and p are defined as vectors. x represents the vector of error motions that may include the measured joint and end-effector displacements, backlashes, or other small unknown displacements. k represents the number of measurements taken for each pose. p represents the vector of parameters in the error model to be estimated. n denotes the unknown number of parameters. m denotes the number of constraints or loops. $k \geq m$ and $(\partial f/\partial x) = m$ must be satisfied to guarantee that the loop can always be closed. The robot moves as the designed fixed-loop motion, and measurements of x for each pose are obtained. For a particular pose i, let us assume that the true value of the measurement vector is x_i, which is recorded as measurement $\overline{x_i}$ with unknown measurement error $\hat{x}_i$ so that $x_i = \overline{x_i} + \hat{x}_i$. Throughout all the sample poses, the parameters should be constant, but our initial estimates of $\bar{p}$ parameters may be in error by $\hat{p}$, that is, $p = \bar{p} + \hat{p}$. For example, in Eq. (7), $\bar{p}$ might be the designed value of a link length and $\hat{p}$ would then be the error incurred in manufacturing the part. Equation (6) becomes

$$f(x_i, p) = f(\overline{x_i} + \hat{x}_i, \bar{p} + \hat{p}) = 0, \quad i = 1, \ldots, N \quad (7)$$

where N represents the number of sample positions. The identification problem then becomes finding the maximum-likelihood estimation of $\hat{p}$. The χ^2 error function is derived as follows:

$$X^2 = \sum_{i=1}^{N} \hat{x}_i^T \sum_x^{-1} \hat{x}_i + \hat{p}^T \sum_p^{-1} \hat{p}$$
$$\sum_x = v_{ar}(\hat{x}) \quad \text{and} \quad \sum_p = v_{ar}(\hat{p}) \tag{8}$$

Σ_x and Σ_p are covariance. If each element of x and p are independent, then Σ_x and Σ_p are taken to be diagonal matrices of variances based on a priori knowledge of the robot and measurement process.

Maximum-likelihood estimation is used to solve this error model and minimize the error by fitting the parameters in Eq. (8). The result of this method is a maximum-likelihood estimate of the model parameters as well as a confidence bound on this estimate. However, there is a challenge to avoid overfitting the model parameters when so many parameters are involved. Also, the uncertainty of robot repeatability and the measurement system needs to be considered. Here, a solution is developed to wrap the implicit loop estimation with the second layer of optimization. That second layer has input vectors of polynomials. The challenging part is developing an efficient cost function for this outer layer of optimization. Because it is a combinatorial problem, there is no concept of a derivative or gradient. Quasi-Newton methods cannot work without the gradient. Every function for evaluation will require at least one run of implicit loop optimization. Iterations to reach convergence may take a lot of time. Moreover, results cannot be evaluated merely by the residual error of the implicit loop because the error gets smaller with more parameters (i.e., higher order polynomials). It might result in overfitting, which leads to bad predictions.

To solve this challenge, a Bayesian information criterion (BIC) [26] penalty function is developed to calculate the BIC score for the multi-output system cost evaluation. It is developed as follows:

$$\text{BIC} = \text{numPts}/2 * \log(\text{detCovR}) + \text{RSS}/2 + K/2 * \log(\text{numPts}) \tag{9}$$

where numPts is the number of measurement poses; DetCovR is the determinant of the covariance of the residuals; RSS is the residual sum of squares where each residual is a single dimension, but all are squared and summed together; and K is the sum of the total number of parameters and number of measured dimensions (for our work, 6). The model with the lowest BIC score is preferred. The optimization starts with the input vector of polynomial orders as the initial guess to calculate a base model. Next, the BIC score is calculated. Then, a polynomial is picked to change. The BIC score is recalculated and compared with the previous BIC score. If the BIC score is lower, then one should accept the change; if the score is higher, one should not accept the change and return to the first step. This process continues until the BIC score cannot be lowered any further in the neighborhood search.

An advanced method to change the picked polynomial is developed using graphics-based optimization. A confidence bound is drawn together with the polynomial. The smaller the BIC score, the tighter fit of the confidence bound with the estimated polynomial. By observing the graph relationship, two criteria are found to guide the change of polynomial parameters. In the beginning, the maximum parameter of a polynomial equation is found. Then, the uncertainty of the polynomial parameters is exposed. The criteria are (1) if any polynomial parameter is smaller than the value of the maximum parameter (for example, lower than 8%), change the polynomial parameter to zero (so the polynomial order is reduced to remove overfitting) and (2) if any polynomial parameter is smaller than the uncertainty value, change the polynomial parameter to zero. After the optimization converges, the χ^2 value needs to be observed to make sure that the model adequately represents the errors of the robot. If the χ^2 is unexpectedly high (e.g., five times higher than the medium number), the most likely problem is either (1) the variance of measurement errors is too high. In this condition, the 7D measurement system needs to be checked. One example of checking the 7D measurement system involves using a calibration artifact to determine the change in the accuracy of the 7D measurement system; or (2) the priori parameter errors have been set too small. It means the initial guessing of the measurement instrument's accuracy is worse than the real condition. The measurement instrument has contributed more errors than expected. The initial value of the instrument uncertainty needs to be adjusted to larger values and the data analysis needs to be rerun.

There are two outputs from the final data analysis. The first one is the derived errors from the calculation of the robot tool center accuracy of the robot through the workspace. Because the uncertainties of the measurements are decoupled from the true errors, the analysis result will not be biased by a measurement system's uncertainty. The second output is to identify the maximum-likelihood estimation of parameters to minimize the error function. This result can be used to identify the root cause of axis errors.

6 Use Case Analysis, Results, and Discussion

A use case was developed under the existing robot platform. The setup is shown in Fig. 5. A UR5 robot is mounted on an optical table. A fixed-loop measurement plan is generated for the UR5 and executed on the robot. The 7D measurement system is used to measure the robot TCP's position and orientation. The 7D measurement system consists of a measurement instrument (a two-camera based stereovision measurement device) and a smart target. The 7D measurement instrument is situated opposite to the UR5 robot as shown in Fig. 5. The smart target (U.S. patent pending) was mounted on the last joint of the UR5 robot. The motor-driven smart target can constantly rotate toward the 7D measurement instrument during the robot motion. The use of smart target enables the nonblocking measurement during robot motion.

Figure 6 shows the distribution of the fixed-loop motion in the joint space and the Cartesian space that is generated for UR5. Hundred and fifty positions were generated as an initial measurement plan as shown in the left picture of Fig. 6. After the fixed-loop generation check, 78 positions passed the checks of the measurement plan and were thereby kept while the remaining 72 positions were discarded. The right picture of Fig. 6 shows the final path of the fixed-loop motion. A script language program is created to run the fixed-loop motion on the UR5. The TCP's position and orientation are measured by the 7D measurement system. Then, an analysis is performed to identify the robot error model using the measured data. To verify the model identification capability and avoid real damage to the robot, some simulated robot joint errors and measurement uncertainty were added to the measurement result to simulate the robot error. Simulated joint errors of J1 were added into the robot error model "E," following the definition in Eq. (1).

There are two outputs from the data analysis. The first output is the derived error from the calculation of the robot tool center

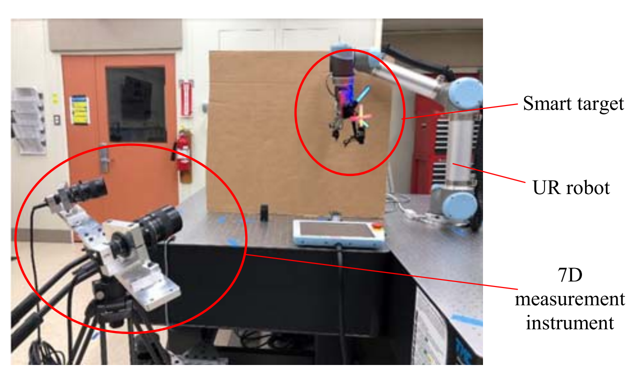

Fig. 5 Use case setup

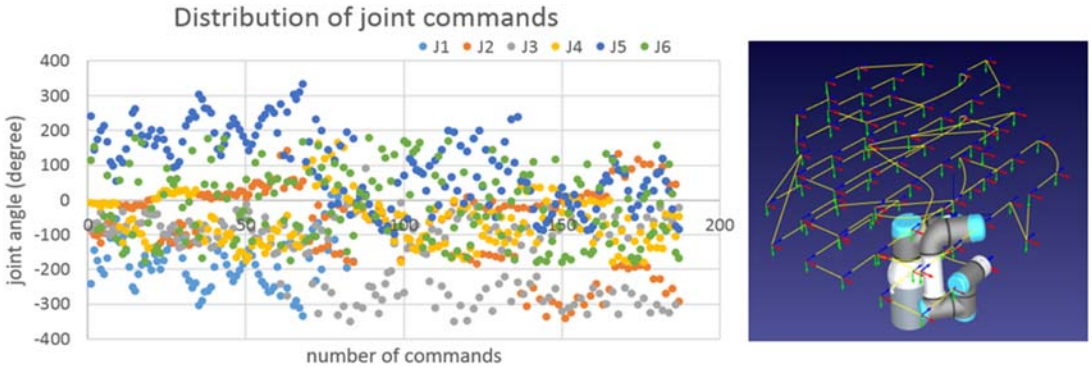

Fig. 6 Even distribution of measurements in the joint space

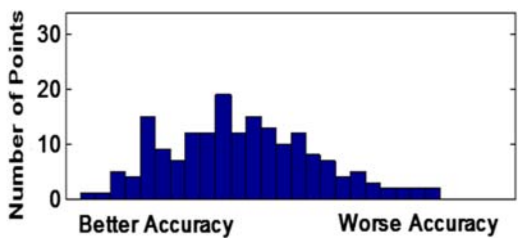

Fig. 7 Robot's error histogram

accuracy of the robot through the workspace. Results include average error, the standard deviation of the error, and maximum error. The accuracy results can help to monitor the change of error distribution, provide a comparison of different robot systems' positional health, and establish a baseline of the robot system's positional health condition. Figure 7 shows the histogram of the error distribution. The results are more accurate because they are derived from the error model instead of directly calculating from the limited size of sample measurements.

The second output is the identified maximum-likelihood estimation of axis error parameters. Figure 8 represents joint 1's position-dependent axis. Following the definition of Eq. (1), the $\delta(\theta)$ and $\varepsilon(\theta)$ in "E" are not constant values; they are a function of joint 1 positions. In graphs shown in Fig. 8, the x-axis represent J1's joint angle range, ranging from −360 deg to 360 deg. J1's three position errors (δ_x, δ_y, and δ_z in x, y, and z directions) and three rotation errors (ε_x, ε_y, and ε_z as pitch, yaw, and roll) are position-dependent errors. For example, ε_z represents angular positioning error of the joint 1 axis. ε_z is also called the scale error of the rotation axis. In this use case, the zero-order constant offset in the ε_z chart denotes that the joint 1's encoder has the error of encoder zero offset.

By observing the shape changes of the identified error model "E," users can monitor the degradation of robot accuracy. Further analysis of the polynomial pattern can be used to identify the potential error sources to create solutions. Given a new set of joint commands, which is different from the measurement plan locations, estimated errors are calculated based on the error model. The programs designed for the robot to perform a task can be evaluated

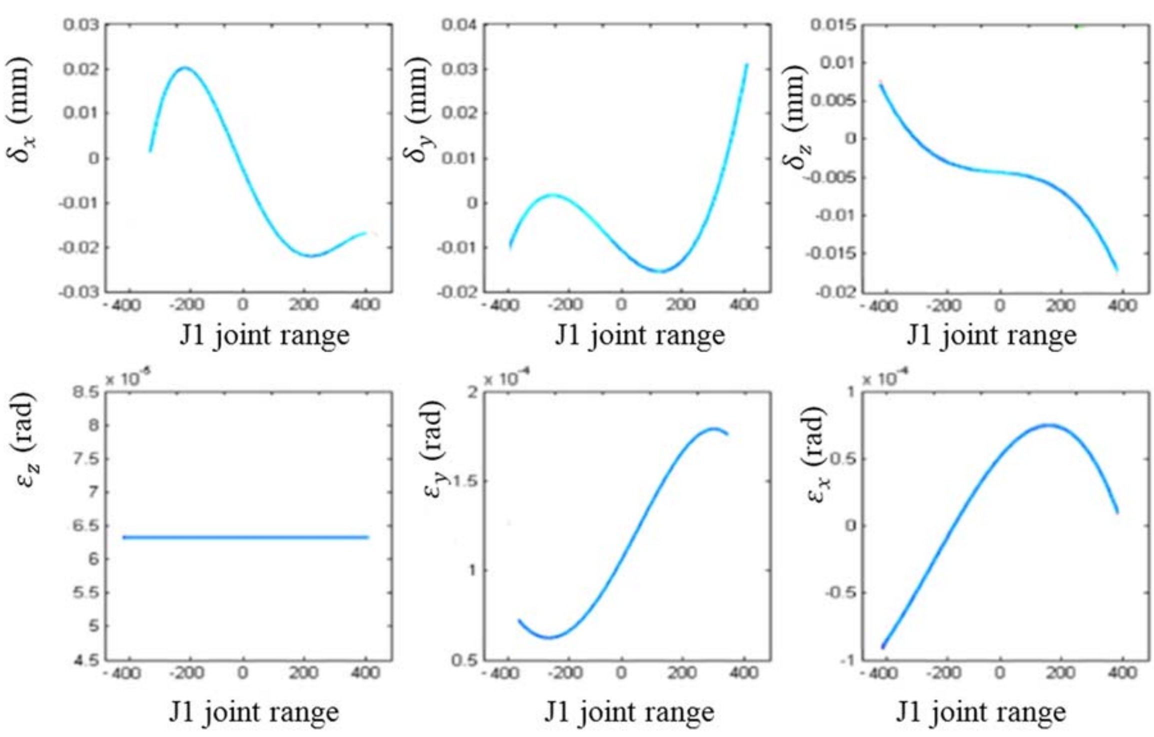

Fig. 8 J1's error distribution

before they are sent to the robot. During the evaluation, if large errors occur at some locations in the commands, adjustments can be made accordingly in the command to correct the errors.

7 Conclusion

NIST's development of the quick health assessment methodology is presented as a means of monitoring industrial robot accuracy degradation. This paper highlights the development of an advanced robot error model that characterizes both robot geometric and nongeometric errors, including the nonideal joint motions and structure/joint deflections. A novel analysis method solves the challenge of decoupling zero-order (constant errors) and high-order (position-dependent) errors. An innovative optimization method is presented to identify the multivariate parameters and to decouple the measurement instrument's uncertainty from actual robot errors.

The methodology provides manufacturers a tool to quickly detect problems in scenarios when environmental conditions change, reconfigurations occur in the work cell, or manufacturers need to ensure that the robot has not experienced a degradation when a critical task is about to be performed in the work cell. The use of this methodology will monitor the degradation of robot performance, reduce scrap and unexpected shutdowns and help optimize maintenance strategies to improve productivity. In support of this effort, NIST is also seeking to develop additional industrial use cases where the quick health assessment methodology can be applied.

7.1 NIST Disclaimer. Certain commercial entities, equipment, or materials may be identified in this document to illustrate a point or a concept. Such identification is not intended to imply recommendation or endorsement by NIST, nor is it intended to imply that the entities, materials, or equipment are necessarily the best available for the purpose.

References

[1] Anandan, T. M., 2016, *Aerospace Manufacturing on Board With Robots*, RIA, Ann Arbor, MI.
[2] Rossmann, J., 2015, "eRobotics Meets the Internet of Things Modern Tools for Today's Challenges in Robotics and Automation," Proceedings 2015 International Conference on Developments in Esystems Engineering Dese 2015, Burj Khalifa, Dubai, UAE, Dec. 12–15, pp. 318–323.
[3] Culla, D., Gorrotxategi, J., Rodriguez, M., Izard, J. B., Herve, P. E., and Canada, J., 2018, "Full Production Plant Automation in Industry Using Cable Robotics With High Load Capacities and Position Accuracy," Robot 2017: Third Iberian Robotics Conference, Vol. 2, Vol. 694, A. Ollero, A. Sanfeliu, L. Montano, N. Lau, and C. Cardeira, eds., Seville, Spain, Nov. 22–24, Springer International Publishing Ag, Cham, pp. 3–14.
[4] DeVlieg, R., 2010, "Expanding the Use of Robotics in Airframe Assembly Via Accurate Robot Technology," SAE Int. J. Aerospace, **3**(1), pp. 198–203.
[5] Kim, H. J., Kawamura, A., Nishioka, Y., and Kawamura, S., 2018, "Mechanical Design and Control of Inflatable Robotic Arms for High Positioning Accuracy," Adv. Rob. **32**(2), pp. 89–104.
[6] Klimchik, A., and Pashkevich, A., 2018, "Robotic Manipulators With Double Encoders: Accuracy Improvement Based on Advanced Stiffness Modeling and Intelligent Control," IFAC Papersonline, **51**(11), pp. 740–745.
[7] Mitsi, S., Bouzakis, K. D., Mansour, G., Sagris, D., and Maliaris, G., 2004, "Off-line Programming of an Industrial Robot for Manufacturing," Int. J. Adv. Manuf. Technol. **26**(3), pp. 262–267.
[8] Yuan, P. J., Chen, D. D., Wang, T. M., Cao, S. Q., Cai, Y., and Xue, L., 2018, "A Compensation Method Based on Extreme Learning Machine to Enhance Absolute Position Accuracy for Aviation Drilling Robot," Adv. Mech. Eng., **10**(3), p. 11.
[9] Shen, N. Y., Guo, Z. M., Li, J., Tong, L., and Zhu, K., 2018, "A Practical Method of Improving Hole Position Accuracy in the Robotic Drilling Process," Int. J. Adv. Manuf. Technol. **96**(5–8), pp. 2973–2987.
[10] Schares, R., Schmitt, S., Emonts, M., Fischer, K., Moser, R., and Fruhauf, B., 2018, "Improving Accuracy of Robot-Guided 3d Laser Surface Processing by Workpiece Measurement in a Blink,," *High-Power Laser Materials Processing: Applications, Diagnostics, and Systems VII*, Vol. 10525, S. Kaierle, and S. W. Heinemann, eds., Spie-Int Soc Optical Engineering, Bellingham, 1052508-2.
[11] Drouot, A., Zhao, R., Irving, L., Sanderson, D., and Ratchev, S., 2018, "Measurement Assisted Assembly for High Accuracy Aerospace Manufacturing," IFAC Papersonline, **51**(11), pp. 393–398.
[12] Massi, F., Bouscharain, N., Milana, S., Le Jeune, G., Maheo, Y., and Berthier, Y., 2014, "Degradation of High Loaded Oscillating Bearings: Numerical Analysis and Comparison With Experimental Observations," Wear, **317**(1–2), pp. 141–152.
[13] Abdi, H., Nahavandi, S., Frayman, Y., and Maciejewski, A. A., 2012, "Optimal Mapping of Joint Faults Into Healthy Joint Velocity Space for Fault-Tolerant Redundant Manipulators," Robotica, **30**(4), pp. 635–648.
[14] Visinsky, M. L., Cavallaro, J. R., and Walker, I. D., 1994, "Robotic Fault Detection and Fault Tolerance: A Survey," Reliab. Eng. Syst. Saf. **46**(2), pp. 139–158.
[15] Bittencourt, A. C., 2012, "On Modeling and Diagnosis of Friction and Wear in Industrial Robots," Postgraduate thesis, Department of Electronic Engineering, Linköping University, Linköping.
[16] Caccavale, F., Marino, A., Pierri, F., and IEEE, 2010, "Sensor Fault Diagnosis for Manipulators Performing Interaction Tasks," IEEE International Symposium on Industrial Electronics (ISIE 2010), Bari, Italy, July 4–7, pp. 2121–2126.
[17] Caccavale, F., Cilibrizzi, P., Pierri, F., and Villani, L., 2009, "Actuators Fault Diagnosis for Robot Manipulators With Uncertain Model," Control Eng. Pract. **17**(1), pp. 146–157.
[18] Weiss, B. A., Vogl, G. W., Helu, M., Qiao, G., Pellegrino, J., Justiniano, M., and Raghunathan, A., 2015, "Measurement Science for Prognostics and Health Management for Smart Manufacturing Systems: Key Findings From a Roadmapping Workshop," Presented at the Annual Conference of the Prognostics and Health Management Society 2015, Coronado, CA, Oct. 18–24, pp. 46–52.
[19] Rodrigues, L. R., Gomes, J. P. P., Ferri, F. A. S., Medeiros, I. P., Galvao, R. K. H., and Nascimento, C. L., 2015, "Use of PHM Information and System Architecture for Optimized Aircraft Maintenance Planning," IEEE Syst. J. **9**(4), pp. 1197–1207.
[20] Qiao, G. X., and Weiss, B. A., 2018, "Quick Health Assessment for Industrial Robot Health Degradation and the Supporting Advanced Sensing Development," J. Manuf. Syst. **48**(Part C), pp. 51–59.
[21] Jang, J. H., Kim, S. H., and Kwak, Y. K., 2001, "Calibration of Geometric and Non-Geometric Errors of an Industrial Robot," Robotica, **19**(3), pp. 311–321.
[22] Qiao, G., and Weiss, B. A., 2017, "Accuracy Degradation Analysis for Industrial Robot Systems" Proceedings of 2017 ASME International Manufacturing Science and Engineering Conference, Los Angeles, CA, June 4–8, University of Southern California, Los Angeles, CA, MSEC2017-2782.
[23] Zhang, X. P., Yan, W. C., Zhu, W., and Wen, T., 2012, *Applied Mechanics and Civil Engineering*, Vol. 137, R. Zhu, ed., Trans Tech Publications Ltd, Zurich, Switzerland, pp. 382–386.
[24] Phillips, F., 2006, "A Novel Means of Software Compensation for Robots and Machine Tools," SAE Technical Paper 2006-01-3167.
[25] Sammons, P. M., Ma, L., Embry, K., Armstrong, L. H., Bristow, D. A., and Landers, R. G., 2014, *Modeling and Compensation of Backlash and Harmonic Drive-Induced Errors in Robotic Manipulators*, Amer Soc Mechanical Engineers, New York.
[26] Ma, L., Bazzoli, P., Sammons, P. M., Landers, R. G., and Bristow, D. A., 2018, "Modeling and Calibration of High-Order Joint-Dependent Kinematic Errors for Industrial Robots," Rob. Comput. Integr. Manuf., **50**, pp. 153–167.
[27] Kalvodova, P., and Zalud, L., 2018, "Accuracy Evaluation Method of Multispectral Data Fusion for Robotic Systems," *Modelling and Simulation for Autonomous Systems*, Vol. 10756, J. Mazal, ed., Springer International Publishing Ag, Cham, pp. 237–250.
[28] Wampler, C. W., Hollerbach, J. M., and Arai, T., 1995, "An Implicit Loop Method for Kinematic Calibration and Its Application to Closed-Chain Mechanisms," IEEE Trans. Rob. Autom. **11**(5), pp. 710–724.